Bottom-Up Assembly of Multicomponent Coordination-Based Oligomers

ARTICLE *in* THE JOURNAL OF PHYSICAL CHEMISTRY C · JULY 2011

Impact Factor: 4.77 · DOI: 10.1021/jp201339p

THE JOURNAL OF PHYSICAL CHEMISTRY C

ARTICLE

pubs.acs.org/JPCC

Bottom-Up Assembly of Multicomponent Coordination-Based Oligomers

Prakash Chandra Mondal,[†] Jeyachandran Yekkoni Lakshmanan,[‡] Hicham Hamoudi,[‡] Michael Zharnikov,[*,‡] and Tarkeshwar Gupta[*,†,‡]

[†]Department of Chemistry, University of Delhi, Delhi −110 007, India

[‡]Lehrstuhl für Angewandte Physikalische Chemie, Universität Heidelberg, Germany

Supporting Information

ABSTRACT:

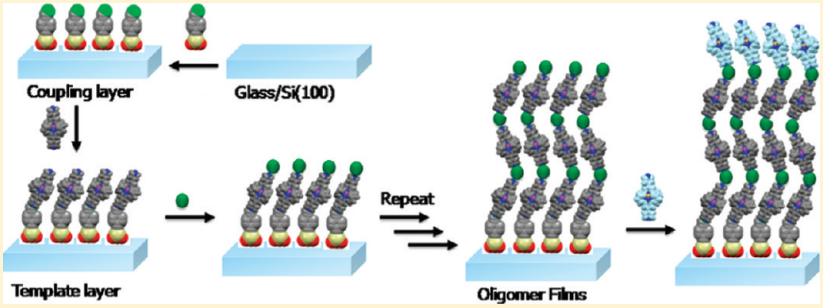

Transition metal complexes allow a high degree of molecular design flexibility through symmetry considerations and ligand architecture, which can be explored for the fabrication of ordered multilayer assemblies through bottom-up approach. Here we describe the preparation of such assemblies, viz. multicomponent coordination-based oligomer films on siloxane-based templates by wet-chemical layer-by-layer deposition process. In these films we combined optically rich iron and ruthenium polypyridyl complexes having pendant pyridine groups (so-called metallo-ligands) and a coinage metal (copper or silver) that acted as a linker between the polypyridyl complex moieties. The properties and structural parameters of the primary template and the oligomer films were studied by X-ray photoelectron spectroscopy, near-edge X-ray absorption fine structure spectroscopy, UV−vis spectroscopy, spectroscopic ellipsometry, atomic force microscopy, and contact angle goniometry. A linear increase in the film thickness upon addition of every next layer suggests that the long-range order of the system is determined by the octahedral structure of the metallo-ligand and square-pyramidal/tetrahedral geometry of the coinage metal linker. Spectroscopic data indicate the existence of electronic communication throughout the individual metallo-organic chains.

1. INTRODUCTION

Coordination polymers (CPs)[1,2] and metal−organic frameworks (MOFs)[3−6] represent a class of advanced inorganic−organic hybrid materials with well-defined coordination between metal and organic linker. A proper choice of the latter elements enables the fabrication of a wide variety of metallosupramolecular architectures.[7−11] During past few decades assembly of CPs and MOFs as bulk materials has experienced a research boom. However, fabrication of coordination-based oligomers and polymers on a solid support remains a challenge so far.[12−16] In particular, the growth of surface-confined coordination oligomers (COs) or CP materials and their structural properties are often difficult to predict and perform in a controlled way since it is affected by a variety of different factors including the efficiency of coordination chemistry, intermolecular interactions, etc.

The majority of the CP films described in the literature[13] have been grown by immersion of selected substrates (silica, alumina, graphite, etc.) into specifically pretreated solvothermal mother liquors of particular CP precursors (usually organic linkers and metal salts). On the other hand, an alternative procedure, viz. a wet-chemical stepwise assembly of well-defined multilayer from a given set of components becomes more and more popular for the fabrication of new CO or CP films.[17−22] The main advantage of this approach is that the chemical and physical properties of the resulting materials can be programmed in advance through smart design of the building blocks; also the mechanistic and kinetic monitoring of the CPs growth can be performed in more details from a new perspective. Furthermore, the layer-by-layer method offers a unique opportunity to grow well-defined heterometallic, multicomponent coordination-based oligomers (MCOs) or polymers (MCPs), which might be difficult to achieve by established solvothermal routes.[14] For instance, the deposition of CPs with alternating layers (heterostructures), possibly with nonperiodic combinations of different metal ions and/or different linkers (herein optically rich and redox-active "metallo-ligands") should be practicable and useful for many applications including gas/metal sensing,[23,24] data storage,[25] electro-chromic materials,[26] etc. In this context, various coordination-based,

Received: February 10, 2011
Revised: June 16, 2011
Published: July 18, 2011

Scheme 1. Molecular Structure of the Metallo-Ligands 1 and 2, M = Ru (1) or Fe (2)[a]

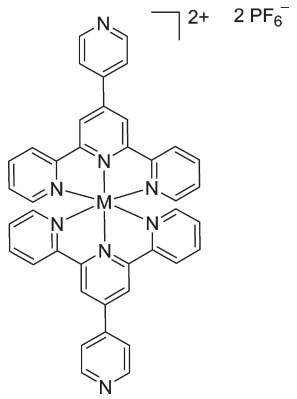

[a] These metallo-ligands were characterized by ^{1}H NMR, UV-vis spectroscopy, and mass spectrometry (see the Supporting Information).

metal−organic multilayer assemblies involving different organic ligands and metals (i.e., zirconium, zinc, palladium, or iron) have been prepared and studied.[19,27,28] A representative example of such an assembly is a homometallic, molecular-wire-like structure combining trispyridyl organic moiety and iron metal, which was reported by Rampi et al. recently.[29] However, a combination of metallo-ligands and coinage metals, such as copper or silver, within a CP or MCO architecture is relatively rare.[30,31] This is an essential drawback since, contrary to the pure organic ligands as a precursor for CP or MCO fabrication,[31] the use of metallo-ligands may provide numerous advantages such as enhanced optical properties, robustness of the system, multiple coordination sites, flexible geometric control, the possibility to assemble a heterometallic system, incorporation of amplified photophysical properties, etc. Among these options, the possibility to assemble a heterometallic system is probably most interesting since such a system may serve as a versatile platform for multibit data storage. For this purpose, such a system should be assembled on a solid support.

In this context, we report here solution-based layer-by-layer assembly of multicomponent, coordination-based molecular wire film in which constituents two different metallo-ligands (Scheme 1) are linked together by $Cu(NO_3)_2$ or $AgNO_3$ moieties. The wires are arranged in an upright zigzag fashion on SiO_x substrate. As representative metallo-ligands we selected well-known, robust, optically rich, and structurally well-defined polypyridyl ruthenium and iron chromophores **1** and **2** (Scheme 1) which have two pendant pyridine moieties (so-called metallo-ligands). The latter moieties react readily with the coinage metals (Cu^{2+} or Ag^+), forming $(RC_5H_4N)_2Cu(NO_3)_2(S)$ or $(RC_5H_4N)_2Ag(NO_3)(S)$ complexes (S = CH_3CN or H_2O). Further, the solvent attached to the metal center could be easily removed at elevated temperature, and the resulting, unsaturated metal center might be useful possessing interesting properties related to host−guest chemistry, sensing, and storage.

2. RESULTS AND DISCUSSION

The known metallo-ligands **1** and **2** were chosen for this study because of their octahedral geometry with the linearly positioned free pendant pyridine groups[32] that could allow for the formation of a 1D chain with coinage metals such as Ag(I) and/or Cu(II). The fabrication of coordination-based oligomer assembly is based on a combination of square pyramidal/tetrahedral geometry of Cu(II) and Ag(I) along with trans positioning of the pyridine ligands. This metal−ligand combination has been utilized extensively by Constable et al.[33−35] to generate 1D and 2D coordination polymer in solid-state materials. In the present study, multicomponent, metal−organic, chain-like structures were fabricated on functionalized glass and silicon substrates (Scheme 2; see below for a detailed description).

Freshly cleaned[24] (see the Supporting Information) glass and silicon substrates (25 mm × 10 mm × 1 mm) were functionalized by immersion in a dry *n*-pentane solution of trichloro-(4-chloromethyl-phenyl)-silane (0.1 mM) at room temperature for 20 min under nitrogen atmosphere. Further, the metallo-ligand **1** was used for the formation of pyridine-terminated template layer. The template layer was formed by reacting chloro-terminated coupling layer with **1** in acetonitrile/toluene (1:1 v/v) solution (0.5 mM) at a temperature of 80 °C for 52 h in a sealed ace glass pressure vessel under N_2 with exclusion of light. The prolonged reaction time did not increase optical absorption, which indicated the completeness of the template layer formation. Note that these layers adhered strongly with the SiO_x substrates and were stable for months under dark and ambient conditions as judged by UV−vis spectroscopy. Neither washing with common solvent nor mechanical abrasion could remove the film. In addition, the template layer exhibited excellent thermal stability up to 200 °C as judged by UV−vis spectroscopy at elevated temperatures (Figure S2), which is common for polypyridyl metal complexes.[36]

The template layer was characterized by UV−vis spectroscopy, X-ray photoelectron spectroscopy (XPS), near-edge X-ray absorption fine structure (NEXAFS) spectroscopy, spectroscopic ellipsometry, contact angle (CA) goniometry, and tapping mode atomic force microscopy. The UV−vis spectrum of the template layer on glass substrate shows the characteristic metal-to-ligand charge-transfer (MLCT) band at λ_{max} = 498 nm. This feature is comparable to the analogous band in the UV−vis spectrum of **1** in solution with red shift of $\Delta\lambda$ = +9 nm. The average molecular density of the template layer **1** was estimated at 1.8×10^{14} cm^{-2} (~55 Å^2/metallo-ligand) from the optical data assuming that the molecular extinction coefficient (ε) of the layer is similar to that observed in solution ($\varepsilon \approx 31167$ cm^{-1} M^{-1} at λ = 490 nm) for the MLCT band. This is in good agreement with the previously reported density values of uniform osmium-polypyridyl-complex-based monolayers.[37] In support of the UV−vis data, which assumed the formation of well-defined template layer, tapping-mode AFM image of this film showed a relatively smooth film surface with no apparent features such as e.g., islands, grains or defects. Root-mean-square (rms) roughness, R_{rms} measured for 1000 nm × 1000 nm scan areas was found to be ~0.40 nm (Figure S1). The CA measurements showed a rather hydrophobic surface with $\theta = 78 \pm 6°$. XPS spectra of the template layer (see Figure 1) showed the clear signatures of Ru at 281.4 eV (Ru $3d_{5/2}$) and the pyridine nitrogen at 400.4 eV as could be expected from the molecular composition of **1** (the binding energy scale was calibrated to the Si2p peak at 99.15 eV).[38]

The ellipsometry-derived thickness of the template layer was estimated at 18.00 ± 0.5 Å, whereas the analogous synchrotron high-resolution XPS-derived value was 19.2 ± 0.40 Å. Notably, the length of metallo-ligand **1** as determined by single crystal

Scheme 2. Schematic Representation of the Wet Chemical Layer-by-Layer Deposition of the Target Coordination-Based Oligomer Assembly[a]

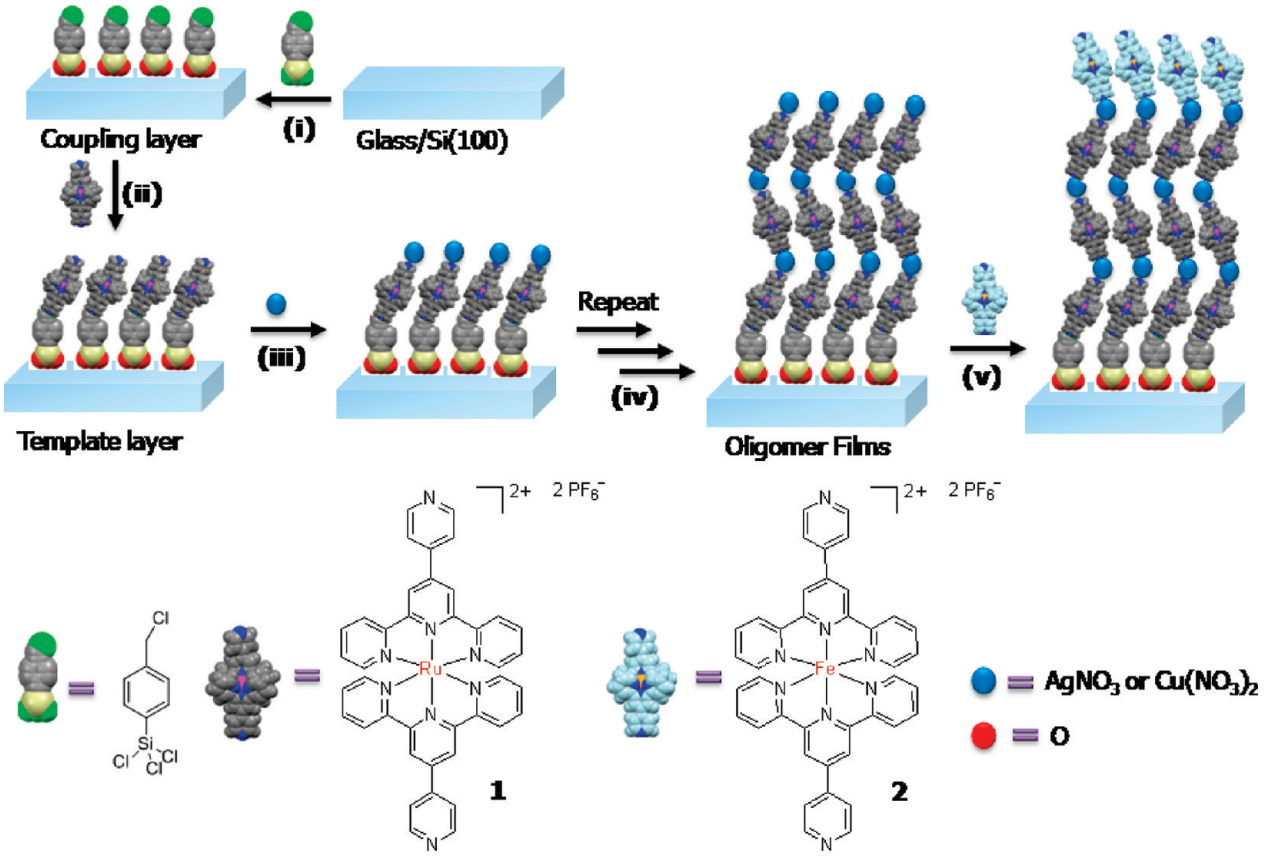

[a] (i) Chemisorption of trichloro-(4-chloromethyl-phenyl)-silane on hydrophilic substrates to form a "coupling layer"; (ii) covalent assembly of the metallo-ligand **1** from acetonitrile solution (0.5 mM) to form a "template layer"; (iii) coordination of silver/copper nitrate with the terminal pyridyl groups of the template layer; (iv) repetition of the steps (ii) and (iii); and (v) coordination of the metallo-ligand **2** with the metal-terminated oligomers. The film formation has been carried out in the dark at room temperature and ambient conditions. The counter anions and bound solvents present in the lattice are omitted for clarity.

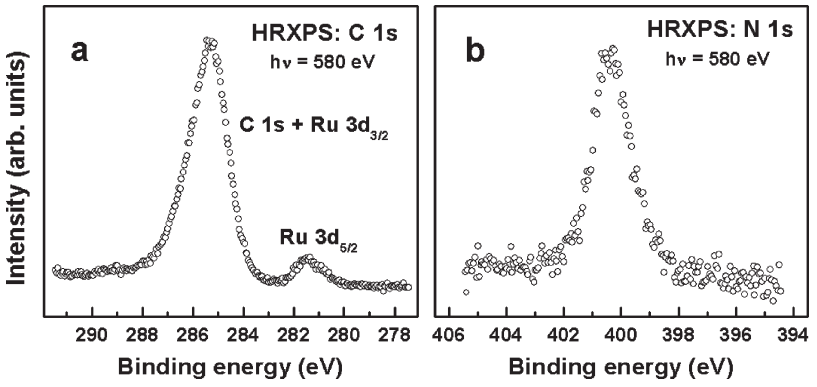

Figure 1. C1s/Ru3d (a) and N1s (b) XPS spectra of the template layer **1** acquired at the synchrotron. Some of the characteristic peaks are marked. The Ru $3d_{3/2}$ peak is merged with the C 1s emission.

X-ray crystallography[32] is 18.3 Å whereas the length of metallo-ligand **1** including trihydroxy(4-chloromethyl-phenyl)-silane (as determined by the Chem3D Pro energy minimization model) is 24.12 Å which is somewhat longer (~5.6 Å) than the experimental XPS and ellipsometer-derived thickness values. This shows that the metallo-ligand **1** is not standing straight-up but slightly (~30°) tilted to the surface. An occurrence of the molecular tilt was also confirmed by the NEXAFS data which are presented in Figure 2.

Both C and N K-edge NEXAFS spectra of the template layer **1** exhibited a characteristic resonance structure of pyridine, viz. a pronounced double $1\pi^*$ resonance at 284.7 and 285.5 eV at the

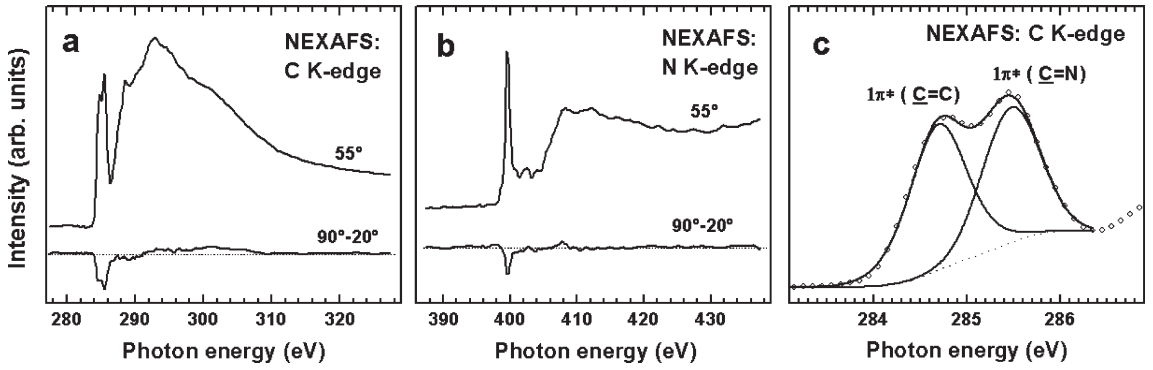

Figure 2. C (a) and N (b) K-edge NEXAFS spectra of the template layer **1** immobilized on functionalized silicon substrate, along with an amplification of the π^* resonance range for the C K-edge spectrum (c). In (a) and (b) both the spectrum acquired at the magic X-ray incidence angle (55°; the spectrum is not affected by orientational effects)[39] and the difference between the spectra acquired at X-ray incidence angles of 90° and 20° are shown.

C K-edge and a strong π^* resonance at 399.6 eV at the N K-edge.[40,41] The splitting of the $1\pi^*$ resonance at C K-edge as compared to benzene, for which only a single $1\pi^*$ resonance at 285.0 eV is observed,[40] is related to the different C1s core level binding energies for the carbon atoms in the ortho positions (C═N) and those in the meta and para positions (C═C) of the pyridine ring.[41] Beyond the characteristic resonances, the NEXAFS spectra of the template layer **1** exhibit a pronounced linear dichroism,[39] i.e., a dependence of the absorption resonance intensity on the angle of X-ray incidence. This dependence, which assumes an orientational order within the template layer, is highlighted by the difference between the spectra acquired at X-ray incidence angles of 90° and 20°. Using a standard theoretical framework[39] and the entire set of the NEXAFS spectra acquired at different angles of X-ray incidence, an average tilt angle of the molecular backbone of **1** with respect to the surface normal could be estimated at ~41°. We believe, however, that this value is an overestimate and the real tilt angle of the molecular backbone is much smaller. The high value of the average tilt angle obtained in our analysis is related to the torsion of the different aromatic rings with respect to the molecular plane; a distribution of the different torsions makes an impression of a larger tilt.

The above, well-defined template layer was used for the fabrication of the coordination-based oligomer films by an iterative wet-chemical layer-by-layer deposition method as shown in Scheme 2. In short, the template layer was immersed for 30 min in 0.5 mM $Cu(NO_3)_2$ or $AgNO_3$ solution in acetonitrile/water (5:2 v/v) at room temperature. The resulting samples were sonicated at a frequency of 20 kHz using aqueous clearing ultrasonic bath (at room temperature) twice in acetonitrile and once in water for 3 min in each step followed by drying under an N_2 stream. Subsequently, the samples were immersed for another 30 min in a 1 mM solution of the metallo-ligand **1** in acetonitrile/water (5:2 v/v) at room temperature and then sonicated twice in acetonitrile followed by drying under an N_2 stream. These two deposition steps were repeated up to 9 times each, followed by the attachment of the metallo-ligand **2** which terminated the resulting oligomers. The growth of the oligomer films has been monitored by conventional UV−vis spectrophotometry and spectroscopic ellipsometry after each deposition step. The structure and properties (microstructure regularity, composition, wettability, refraction, packing density and interfacial roughness) of these new assemblies were elucidated by means of AFM, XPS, and static CA goniometry.

The UV−vis measurements of the coordination-based assembly in transmission mode showed a good linear correlation between the optical absorption and the number of the metallo-ligand units (see the inset of Figure 3). This suggests the formation of regular oligomer films with a uniform density of both components comprising the repeating units of each oligomer. It is noteworthy that the attachment of one coinage metal moiety and one metallo-ligand-terminated moiety to each oligomer are considered as one cycle which includes two deposition steps. The absorption intensity of the metallo-ligand **1** in the range λ = 400−800 nm did not noticeably change upon deposition of $Cu(NO_3)_2$ or $AgNO_3$. However, a progressive blue shift in λ_{max} with each additional immersion cycle for the Cu-based assembly from λ = 498 nm for the template layer to λ = 479 nm for the 9-fold oligomer film indicated a coordination of Cu^{2+} ion with the pendant pyridyl group as a result of square pyramidal geometry[33] and possible $\pi-\pi$ interactions between the intermolecular wires. This shift was negligible in the case of the Ag-based assembly indicating a lack of the $\pi-\pi$ interactions between the intermolecular wires, which could be due to tetrahedral symmetry considerations.[32] Note that the solid state crystallographic data revealed that the two pyridine donors of similar metallo-ligands bound to copper center are aligned trans to one another and the N−Cu−N unit is closer to be linear (N−Cu−N angle is ~166°)[33] than the N−Ag−N one (N−Ag−N angle is ~150°).[32] The optical absorption, ΔA ~ 0.008 for each metal/metallo-ligand unit is constant and slightly less than that for the template layer (0.0095). The deposition of **2** as the top unit (unit 10) of the oligomer assembly resulted in a red shift ($\Delta\lambda$ = +11 nm) of the absorption maxima in the optical spectrum in the case of the Cu-based assembly, which indicates an electronic communication between the individual components along the metallo-organic chain. However, this shift was not observed in the case of the Ag-based assembly for which the wavelength position of the absorption maximum remained constant at λ_{max} = 490 nm even after the deposition of the top unit. Interestingly, the oligomer film growth could be bunged chemically at any stage by quaternizing the topmost pendant pyridyl group. In particular, immersion of the metallo-ligand-terminated 7-fold oligomer film in 1.00 mM of HCl in H_2O at room temperature or template layer in 1.00 mM of CH_3I in acetonitrile at elevated temperature (~60 °C) resulted in protonation or methylation of the free pyridine group, respectively; thereafter no further growth of the oligomers was observed as judged by

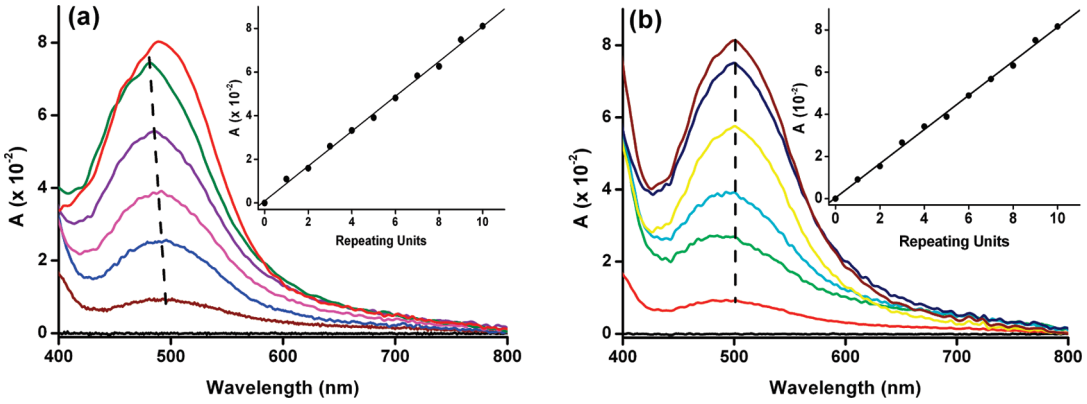

Figure 3. UV−vis absorption spectra of the Cu- (a) and Ag- (b) based metallo-ligand terminated oligomer assemblies (1, 3, 5, 7, 9, and 10 repeating metal/metallo-ligand units - layers). The oligomer films 1−9 are comprised of the **1**-based metallo-ligand, whereas the topmost 10th unit of the oligomers is the metallo-ligand **2**. The **1**-based template layer is defined as step 1. Insets: Absorption (at λ_{max} = 498 to 479 nm for the Cu-based assembly and at λ_{max} = 498 for the Ag-based assembly) vs number of the repeating metal/metallo-ligand units (layers) in the metallo-ligand-terminated oligomers deposited on the glass substrates after baseline correction (R^2 = 0.98 for both system). UV−vis spectra of the metal terminated layer are not shown.

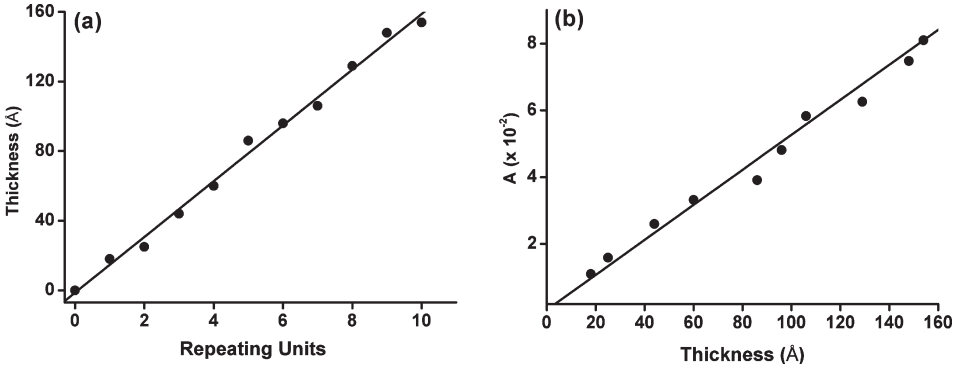

Figure 4. (a) Ellipsometry-derived thickness of the oligomer film on silicon versus the number of the repeating metal/metallo-ligand units (layers) in the metallo-ligand-terminated oligomers. (b) Absorption intensities at λ = 498 nm for the Cu-based oligomer assembly on glass versus the ellipsometry-derived thickness on silicon. The lines are linear fits with R^2 > 0.98.

UV−vis spectroscopy (Figure S3). Remarkably, a red shift ($\Delta\lambda$ = +6 nm) of MLCT band at λ_{max} = 498 nm was observed after protonation or methylation of the film.

The successive film growth was further confirmed by the plot of the ellipsometry-derived thickness as a function of the number of the deposition steps (Figure 4). UV−vis and ellipsometry measurements showed the same stepwise and linear trends, as is evident from the good correlation (R^2 > 0.98) between the absorption intensity and the film thickness during buildup on glass/silicon substrates. The refractive index n of the assembly is within the range of 1.5−1.8. The film thickness was ∼15 nm after 10 deposition cycles. The average thickness increase after each deposition cycle is therefore ∼1.5 nm; which is somewhat smaller than the length of the metallo-ligand 1 determined on the basis of X-ray crystallography data (∼1.9 nm).[32] The increase in thickness due to incorporation of copper or silver metal is additive. This discrepancy in thickness data suggests that the growth of oligomer occurred not perfectly upright (linearly) but in the zigzag fashion as schematically shown in scheme 2. Moreover, the XPS and NEXAFS-derived tilt angle (∼30−40°) for the 1-based monolayer (vide supra) and proposed square planar/tetrahedral geometry around the copper or silver metal atoms also entails the zigzag propagation of the oligomer.

The formation of the oligomer films was also confirmed by XPS as demonstrated by Figure 5, where some of the relevant XPS spectra are shown. In particular, in accordance with the expected chemical composition and architecture of these films, the N1s XPS spectrum of the metallo-ligand **1**-terminated Cu-based oligomer film exhibits a characteristic emission at 400.3 eV related to the coordinated (with Ru^{2+}) pyridine group (N), a weaker signal at 402.8 eV associated with the pyridine group (N*) coordinated with Cu^{2+}, and a pronounced peak at 406.2 eV assigned to the NO_3 group (NO^{2-}) of Cu nitrate respectively. Further, the spectra of the $AgNO_3$ and $Cu(NO_3)_2$ terminated oligomer films showed the characteristic emissions of these metals in +1 and +2 oxidation states, respectively.

The surface morphology of the oligomer films formed on silicon substrates was imaged by tapping mode AFM. Representative images of the metal-terminated and **1**-terminated 5-fold and 6-fold oligomer films are shown in Figure 6. The surface morphology and the root-mean-square roughness (R_{rms} = 0.3 − 0.7 nm for 1000 × 1000 nm^2 scan area) are similar to or better than those for other assemblies[42−44] grown by same methodology on silicon substrates. No great differences between the **1**-terminated and metal-terminated oligomer films were observed. However, the **1**-terminated oligomer films showed a smother surface as compared to the metal-terminated ones.

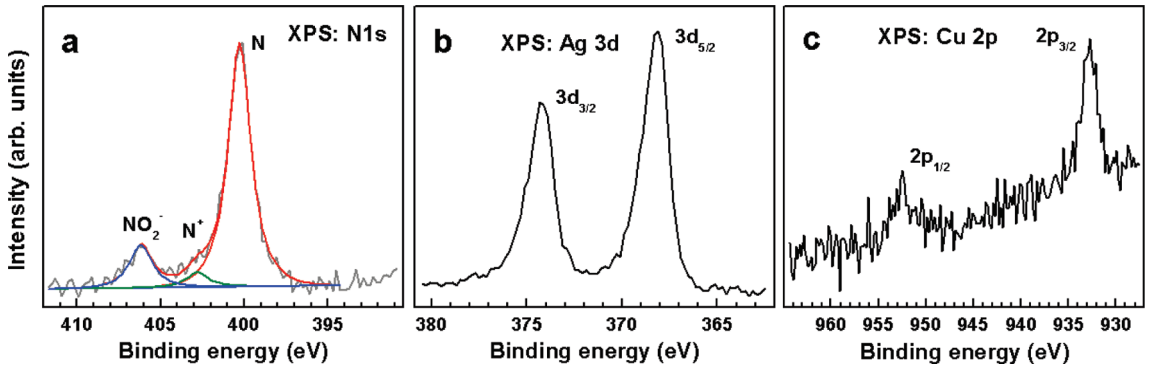

Figure 5. N1s XPS spectrum of metallo-ligand **1**-terminated Cu-based oligomer film (a), along with the Ag 3d spectrum of the $AgNO_3$ terminated oligomer film (b), and the Cu 2p spectrum of the $Cu(NO_3)_2$ terminated oligomer film (c). The characteristic emissions are marked. The experimental N 1s spectrum (gray line) is decomposed into the contributions related to the coordinated (with Ru^{2+}) pyridine group (N; red line), the pyridine group (N*; green line), and the NO_3 group (NO^{2-}; blue line).

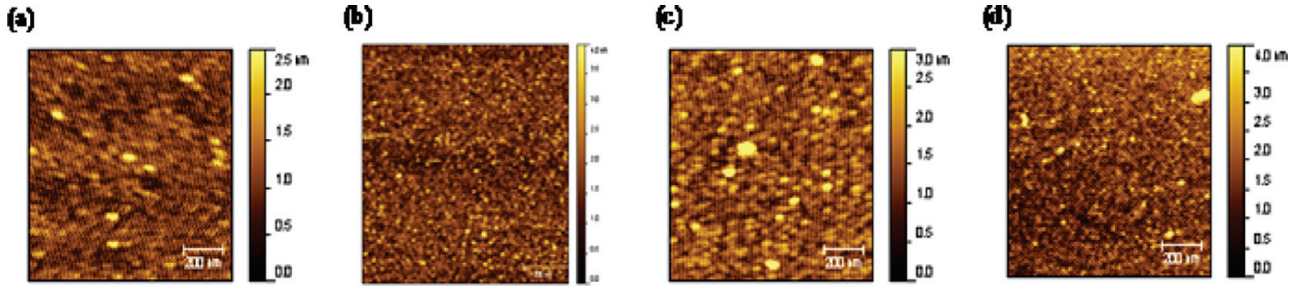

Figure 6. Representative tapping mode AFM images of (a) **1**-terminated $Cu(NO_3)_2$-based 5-fold oligomer film (R_{rms} = 0.36 nm); (b) metal-terminated $Cu(NO_3)_2$-based 6-fold oligomer film (R_{rms} = 0.61 nm); (c) **1**-terminated $AgNO_3$-based 5-fold oligomer film (R_{rms} = 0.45 nm), and (d) metal-terminated $AgNO_3$-based 6-fold oligomer film (R_{rms} = 0.57 nm). The scan area was 1000 × 1000 nm.

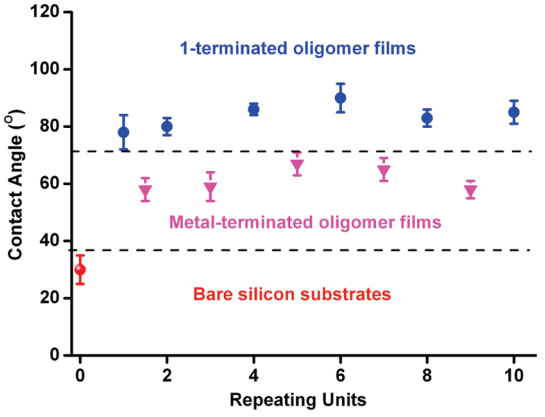

Figure 7. Static aqueous contact angle vs number of the repeating metal/metallo-ligand units (layers) in the metallo-ligand-terminated oligomers with standard deviation error bars (three readings with the same setup but from different areas). Layer "0" indicates the contact angle of the bare silicon substrate used for the oligomer film preparation.

Static aqueous contact angle measurements of the oligomer films on silicon substrates showed a pronounced difference between the metal-terminated and metallo-ligand-terminated oligomer assemblies (Figure 7). However, within either metal- or metallo-ligand termination, no change in contact angle was observed upon the successive growth of the oligomers. This suggests that both chemical composition and roughness were successfully reproduced in the course of the oligomer growth, resulting in a structurally homogeneous assembly. As shown in Figure 7, the static contact angles for the metal- and metallo-ligand-terminated oligomer films were 65 ± 7° and 85 ± 5°, respectively, indicating, as expected that the metallo-ligand-terminated oligomer films were more hydrophobic than the metal-terminated ones. Note that the standard deviation of the contact angle values for each individual film was found to be ±5°.

3. CONCLUSIONS AND OUTLOOK

Surface-initiated LBL-assembly has been used to fabricate heterometallic, multicomponent, coordination-based oligomer (MCOs) films on SiO_x substrates. The oligomers consisted of the terpyridine-Ru/Fe-terpyridine metallo-ligands which were connected by copper or silver nitrate linkers. The Cu- or Ag-pyridine coordination did not only create an excellent structural directing unit but also allowed the incorporation of two different metallo-ligands having identical binding motif. The rigid nature and distinct geometry of the molecular components are well-suited to form molecular-wire-like structure on SiO_x-based surfaces. Moreover, the oligomer growth can be discontinued at any stage by quaternizing the terminal pyridyl group with addition of 1.00 mM of H^+ or CH_3I.

The further work will include controlled alternate assembly of the Ru and Fe trispyridyl moieties and their electrochemical characterization. The use of two functionally different metallo-ligands might allow one to generate multifunctional stimuli-

responsive coordination-based oligomer/polymer materials. Further, temperature-controlled generation of unsaturated metal site in the lattice might make this system valuable candidate for host−guest chemistry.

■ ASSOCIATED CONTENT

Supporting Information. Synthetic details of metalloligands **1** and **2**. Formation, thermal stability test, and AFM image of template layer (Figure S1 and S2). Assembly of multicomponent coordination-based oligomers and its chemical retardation properties (Figure S3). This material is available free of charge via the Internet at http://pubs.acs.org.

■ AUTHOR INFORMATION

Corresponding Author

*(M.Z.) Phone: +49-6221-54 4921. Fax: +49-6221-54 6199. E-mail: Michael.Zharnikov@urz.uni-heidelberg.de. (T.G.) Phone: +91-11-27666646-125. Fax: +91-11-27667794-125. E-mail: tgupta@chemistry.du.ac.in.

■ ACKNOWLEDGMENT

This research was supported by the Department of Science and Technology (DST), Department of Science and Technology-Nano Mission (DST-Nano Mission) and University of Delhi, Delhi. T.G. thanks the Alexander von Humboldt (AvH) foundation for the Humboldt fellowship of experienced researcher. M.Z. thanks M. Grunze for the support of this work, Ch. Wöll and A. Nefedov (KIT) for the technical cooperation at BESSY II, and BESSY II staff for the assistance during the experiments. P.C.M. thanks the council of scientific and industrial research for a junior research fellowship.

■ REFERENCES

(1) Welte, L.; Calzolari, A.; Di Felice, R.; Zamora, F.; Gomez-Herrero, J. *Nat. Nanotechnol.* **2010**, *5*, 110.
(2) Kitagawa, S.; Kitaura, R.; Noro, S.-i. *Angew. Chem., Int. Ed.* **2004**, *43*, 2334.
(3) Tranchemontagne, D. J.; Mendoza-Cortes, J. L.; O'Keeffe, M.; Yaghi, O. M. *Chem. Soc. Rev.* **2009**, *38*, 1257.
(4) Rosi, N. L.; Eckert, J.; Eddaoudi, M.; Vodak, D. T.; Kim, J.; O'Keeffe, M.; Yaghi, O. M. *Science* **2003**, *300*, 1127.
(5) Stuart, J. L. *Chem. Soc. Rev.* **2003**, *32*, 276.
(6) Ma, L.; Falkowski, J. M.; Abney, C.; Lin, W. *Nat. Chem.* **2010**, *2*, 838.
(7) Yaghi, O. M.; O'Keeffe, M.; Ockwig, N. W.; Chae, H. K.; Eddaoudi, M.; Kim, J. *Nature* **2003**, *423*, 705.
(8) Baytekin, H. T.; Baytekin, B.; Schulz, A.; Schalley, C. A. *Small* **2009**, *5*, 194.
(9) Yoshinari, N.; Igashira-Kamiyama, A.; Konno, T. *Chem.—Eur. J.* **2010**, *16*, 14247.
(10) Wang, M.; Zheng, Y.-R.; Ghosh, K.; Stang, P. J. *J. Am. Chem. Soc.* **2010**, *132*, 6282.
(11) Lusby, P. J.; Muller, P.; Pike, S. J.; Slawin, A. M. Z. *J. Am. Chem. Soc.* **2009**, *131*, 16398.
(12) Zacher, D.; Schmid, R.; Woell, C.; Fischer, R. A. *Angew. Chem., Int. Ed.* **2011**, *50*, 176.
(13) Zacher, D.; Shekhah, O.; Woell, C.; Fischer, R. A. *Chem. Soc. Rev.* **2009**, *38*, 1418.
(14) Shekhah, O.; Wang, H.; Paradinas, M.; Ocal, C.; Schuepbach, B.; Terfort, A.; Zacher, D.; Fischer, R. A.; Woell, C. *Nat. Mater.* **2009**, *8*, 481.
(15) Quinn, J. F.; Johnston, A. P. R.; Such, G. K.; Zelikin, A. N.; Caruso, F. *Chem. Soc. Rev.* **2007**, *36*, 707.
(16) Villagomez, C. J.; Sasaki, T.; Tour, J. M.; Grill, L. *J. Am. Chem. Soc.* **2010**, *132*, 16848.
(17) Altman, M.; Rachamim, M.; Ichiki, T.; Iron, M. A.; Evmenenko, G.; Dutta, P.; van der Boom, M. E. *Chem.—Eur. J.* **2010**, *16*, 6744.
(18) Altman, M.; Zenkina, O. V.; Ichiki, T.; Iron, M. A.; Evmenenko, G.; Dutta, P.; van der Boom, M. E. *Chem. Mater.* **2009**, *21*, 4676.
(19) Shi, Z.; Lin, N. *J. Am. Chem. Soc.* **2010**, *132*, 10756.
(20) Greenstein, M.; Ben Ishay, R.; Maoz, B. M.; Leader, H.; Vaskevich, A.; Rubinstein, I. *Langmuir* **2010**, *26*, 7277.
(21) Zhang, X.; Chen, H.; Zhang, H. *Chem. Commun.* **2007**, 1395.
(22) Ariga, K.; Hill, J. P.; Ji, Q. *Phys. Chem. Chem. Phys.* **2007**, *9*, 2319.
(23) Tanaka, D.; Henke, A.; Albrecht, K.; Moeller, M.; Nakagawa, K.; Kitagawa, S.; Groll, J. *Nat. Chem.* **2010**, *2*, 410.
(24) Gupta, T.; Van der Boom, M. E. *J. Am. Chem. Soc.* **2007**, *129*, 12296.
(25) Motiei, L.; Altman, M.; Gupta, T.; Lupo, F.; Gulino, A.; Evmenenko, G.; Dutta, P.; van der Boom, M. E. *J. Am. Chem. Soc.* **2008**, *130*, 8913.
(26) Motiei, L.; Lahav, M.; Freeman, D.; van der Boom, M. E. *J. Am. Chem. Soc.* **2009**, *131*, 3468.
(27) Kaminker, R.; Motiei, L.; Gulino, A.; Fragala, I.; Shimon, L. J. W.; Evmenenko, G.; Dutta, P.; Iron, M. A.; van der Boom, M. E. *J. Am. Chem. Soc.* **2010**, *132*, 14554.
(28) Shekhah, O.; Wang, H.; Strunskus, T.; Cyganik, P.; Zacher, D.; Fischer, R.; Woell, C. *Langmuir* **2007**, *23*, 7440.
(29) Tuccitto, N.; Ferri, V.; Cavazzini, M.; Quici, S.; Zhavnerko, G.; Licciardello, A.; Rampi, M. A. *Nat. Mater.* **2009**, *8*, 41.
(30) Kilduff, B.; Pogozhev, D.; Baudron, S. A.; Hosseini, M. W. *Inorg. Chem.* **2010**, *49*, 11231.
(31) Forster, R. J.; Keyes, T. E. *Coord. Chem. Rev.* **2009**, *253*, 1833.
(32) Beves, J. E.; Constable, E. C.; Housecroft, C. E.; Kepert, C. J.; Price, D. J. *CrystEngComm* **2007**, *9*, 456.
(33) Beves, J. E.; Constable, E. C.; Housecroft, C. E.; Neuburger, M.; Schaffner, S. *CrystEngComm* **2008**, *10*, 344.
(34) Beves, J. E.; Bray, D. J.; Clegg, J. K.; Constable, E. C.; Housecroft, C. E.; Jolliffe, K. A.; Kepert, C. J.; Lindoy, L. F.; Neuburger, M.; Price, D. J.; Schaffner, S.; Schaper, F. *Inorg. Chim. Acta* **2008**, *361*, 2582.
(35) Beves, J. E.; Constable, E. C.; Decurtins, S.; Dunphy, E. L.; Housecroft, C. E.; Keene, T. D.; Neuberger, M.; Schaffner, S.; Zampese, J. A. *CrystEngComm* **2009**, *11*, 2406.
(36) Gupta, T.; Van der Boom, M. E. *J. Am. Chem. Soc.* **2006**, *128*, 8400.
(37) Gupta, T.; Altman, M.; Shukla, A. D.; Freeman, D.; Leitus, G.; Van der Boom, M. E. *Chem. Mater.* **2006**, *18*, 1379.
(38) Moulder, J. F. S., W. E.; Sobol, P. E.; Bomben, K. D. *Handbook of X-ray Photoelectron Spectroscopy*; J. Ed. Perkin-Elmer Corp.: Eden Prairie, MN, 1992.
(39) Stohr, J. *NEXAFS Spectroscopy; Springer Series in Surface Science 25*; Springer-Verlag: Berlin, 1992.
(40) Horsley, J. A.; Stohr, J.; Hitchcock, A. P.; Newbury, D. C.; Johnson, A. L.; Sette, F. *J. Chem. Phys.* **1985**, *83*, 6099.
(41) Kolczewski, C.; Puttner, R.; Plashkevych, O.; Agren, H.; Staemmler, V.; Martins, M.; Snell, G.; Schlachter, A. S.; Sant'Anna, M.; Kaindl, G.; Pettersson, L. G. M. *J. Chem. Phys.* **2001**, *115*, 6426.
(42) Musick, M. D.; Keating, C. D.; Lyon, L. A.; Botsko, S. L.; Pena, D. J.; Holliway, W. D.; McEvoy, T. M.; Richardson, J. N.; Natan, M. J. *Chem. Mater.* **2000**, *12*, 2869.
(43) Sarno, D. M.; Martin, J. J.; Hira, S. M.; Timpson, C. J.; Gaffney, J. P.; Jones, W. E., Jr. *Langmuir* **2007**, *23*, 879.
(44) Man, K. Y. K.; Wong, H. L.; Chan, W. K.; Djurisic, A. B.; Beach, E.; Rozeveld, S. *Langmuir* **2006**, *22*, 3368.